The published version of the paper "E. Fortunati, F. Luzi, A. Jiménez, D. A. Gopakumar, D. Puglia, S. Thomas, J. M. Kenny, A. Chiralt, L. Torre (2016). Revalorization of sunflower stalks as novel sources of cellulose nanofibrils and nanocrystals and their effect on wheat gluten bionanocomposites properties. Carbohydrate Polymers, Carbohydrate Polymers, 149, 357-368" is available at: https://doi.org/10.1016/j.carbpol.2016.04.120.

Revalorization of sunflower stalks as novel sources of cellulose nanofibrils and nanocrystals and their effect on wheat gluten bionanocomposites properties

E. Fortunati[a1], F. Luzi[a], A. Jiménez[b], D. A. Gopakumar [c], D. Puglia[a], S. Thomas [c], J. M. Kenny[a], A. Chiralt[b], L. Torre[a]

[a]*University of Perugia, Civil and Environmental Engineering Department, UdR INSTM, Strada di Pentima 4, 05100 Terni (Italy)*
[b]*Instituto Universitario de Ingeniería de Alimentos para el Desarrollo, Universitat Politècnica de València, Camino de Vera s/n, 46022 Valencia, Spain.*
[c] *International and Inter University Centre for Nanoscience and Nanotechnology, Mahatma Gandhi University, Kottayam, Kerala 686560, India.*

[1]**Corresponding author:** Tel.: +39-0744492921; fax: +39-0744492950; E-mail address: elena.fortunati@unipg.it (E. Fortunati)

Abstract

Novel gluten based bionanocomposites reinforced with cellulose nanofibrils (CNF) and cellulose nanocrystals (CNC) extracted from sunflower stalks by a steam explosion treatment and a hydrolysis procedure, respectively, were prepared by casting/evaporation. The extracted cellulose nanomaterials, both CNC and CNF, were embedded in gluten matrix and their effect was investigated. Morphological investigations highlighted that gluten based bionanocomposites showed a homogenous morphology, the absence of visible cellulose nanoreinforcements, and the

presence of holes for Gluten_CNF nanocomposites. Gluten_CNF showed a reduction of WVP coefficients but the values are higher respect to gluten reinforced with CNC. This behaviour could be related to the ability of CNC to increase the tortuous path of gas molecules. Moreover, the results from thermal, mechanical and barrier properties confirmed the strong interactions obtained between CNC and gluten matrix during the process. The study suggested the possibility to re-valorise agricultural wastes with potential applications as reinforcement in polymer matrix bionanocomposites.

Keywords: Sunflower stalks, cellulose, chemical pre-treatment, steam explosion, hydrolysis, bionanocomposites

1.Introduction

The development and use of green resources represent new objectives for reducing gas emissions and consequent pollution while, in this context, lignocellulosic materials represent renewable resources for production of fuel ethanol from sugars. Among lignocellulosic materials, the use of agricultural residues is of particular interest because it has also the benefit of disposal of problematic solid wastes which usually do not have any economic alternative.

Sunflowers have been considered as one of the major sustainable lignocellulosic materials used not only to extract oils but also for producing biofuels as alternative to fossil fuels (Vaithanomsat, Chuichulcherm & Apiwatanapiwat, 2009; Berglund, 2007). Sunflowers are renewable and are cultivated in large quantities (about 30-35 million metric tons) around the world; while sunflower seeds represent the fourth source of oil in the world, heads, stalks and leaves remain unutilized after harvesting(Ruiz, Cara, Manzanares, Ballesteros & Castro, 2008). These residues are not eco-friendly because after harvesting they are typically burnt under not well-controlled conditions causing a negative environmental impact. Every year, the volume of sunflower residues produced in the world represents a huge environmental impact with 3-7 tonnes of dry matter/ha (Díaz, Cara, Ruiz, Pérez-Bonilla & Castro, 2011; Vaithanomsat, Chuichulcherm & Apiwatanapiwat, 2009.). For these reasons, the attention of the scientific community is now oriented to the revalorization of wastes after sunflower harvesting, and currently the most common use of residual stalks is for bioethanol production (Jung, Yu, Eom & Hong, 2013). However, sunflower residues could be used also as precursors for the extraction of cellulose based materials. Currently, cellulose nanocrystals (CNC) and cellulose nanofibrils (CNF) constitute the two main families of nanosized cellulose. The former is extracted from fibres after a complete dissolution of the non-crystalline fractions, while the latter results from the application of high shearing forces of disintegration leading to a high degree of fibrillation, which yields highly interconnected fibrils. Some different methods are known for the extraction of nanosized cellulosic materials, such as chemical, enzymatical, mechanical

59 treatments, etc.. Among the different existing pre-treatment methods, steam explosion is one of the
60 most commonly used for fractionation of biomass components. In steam explosion pre-treatment,
61 biomass is exposed to pressurized steam followed by rapid reduction in pressure. The treatment
62 results in substantial breakdown of the lignocellulosic structure, hydrolysis of the hemicellulosic
63 fraction, depolymerization of the lignin components and defibration. Compared with alternative
64 pre-treatment methods, the advantages of steam explosion include a significantly lower
65 environmental impact, lower capital investment and less hazardous process chemicals (Chaker,
66 Alila, Mutjé, Vilar & Boufi, 2013).
67 Wheat gluten (WG) protein is an attractive material as agropolymer because of its high availability
68 and it can be easily processed into films (Domenek, Feuilloley, Gratraud, Morel & Guilbert, 2004;
69 Mojumdar, Moresoli, Simon & Legge, 2011). Besides the rapid biodegradability of wheat gluten
70 films, such materials exhibit effective barrier properties against lipids and gases, such as oxygen,
71 carbon dioxide and aroma compounds (Rafieian, F., Shahedi, M., Keramat, J., & Simonsen, J.,
72 2014a). However, the poor mechanical properties and strong water absorption in humid
73 environment of this material tremendously limit the applications in some industrial sectors as
74 packaging. Solving these problems is a key research issue. Some actions have been taken to
75 toughen the polymer matrix through using nanoparticles, for instance montmorillonite (Tunc,
76 Angellier, Cahyana, Chalier, Gontard & Gastaldi, 2007) and cellulose nanofibrils (Rafieian,
77 Shahedi, Keramat & Simonsen, 2014a, b), which are simple and represent an effective way to make
78 a high-performance protein polymer composite.
79 In the present research, we report the use of sunflower stalk wastes as precursors for the extraction
80 of both cellulose nanofibrils (CNF) and cellulose nanocrystals (CNC) to be used as reinforcement
81 phases in wheat gluten natural matrix. The effectiveness of an optimized alkaline pre-treatment
82 followed by an acid hydrolysis was compared with a steam explosion assisted treatment that led the
83 extraction of cellulose nanocrystals and cellulose nanofibrils, respectively. Then, gluten based

bionanocomposites, reinforced with CNC or CNF, were produced by solvent casting in water. Finally, the dispersion of CNF or CNC in wheat gluten matrix, the mechanical response and the thermal and barrier properties of WG nanocomposites reinforced with cellulosic materials were deeply investigated.

2. Experimental

2.1 Materials

Sunflower stalks were collected in Umbria, Italy. The chemical composition of sunflower stalks, expressed in % with respect to dry weight of matter, has been analyzed by many authors (quite wide range of identified values to the variability of growing and harvesting conditions): glucose 27.0 - 36.3%, xylose 16.7- 22.4%, α-cellulose 40.3 - 45.7%; holocellulose 54.0 - 71.85%; lignin 19.5 - 28.1%, ethanol/benzene extractives 5.8 - 16.7%, ash 7.8 - 10.7% (Kopania, Wietecha, & Chiechanska, 2010; Romero, Moya, Cara, Vidal, & Castro, 2013; Akpinar, Levent, Sabanci, Uysal, & Sapci, 2011; Ruiz, Cara, Manzanares, Ballesteros, & Castro, 2008; Khristova, Bentcheva, & Karar, 1998). Glycerol, used as plasticizer, was purchased from Panreac Química (Castellar del Vallés, Barcelona, Spain). Wheat gluten (WG protein content; > 80%, moisture content: 5.5 - 8.0 %) and all chemical reagents were supplied by Sigma Aldrich (Sigma–Aldrich Chemie GmbH, Steinheim, Germany).

2.2 Cellulose nanocrystal extraction

Sunflower stalks were chemically pre-treated before the cellulose nanocrystal (CNC) extraction. Before the chemical pre-treatment, the stalks were washed several times with water and the internal white pith was manually removed. The external fibrous structure was then treated with 5 %wt/v NaOH solution at room temperature (RT) for 72 h (liquid/fibre ratio 30:1) and successively with 5 %wt/v NaOH solution at 98 °C for 2 h (liquid/fibre ratio 10:1). The fibrous structure was also

109 treated with 5%wt/v of sodium chlorite (bleaching fibre/liquid ratio 1:50), boiled for 2 h at pH=4. A
110 treatment with sodium bisulphate solution at 5 %wt/v was then carried out (30 min at RT) and
111 finally a 17.5 % wt/v NaOH solution was applied (20 min at RT) (see Figure 1, Panel A).
112 Cellulose nanocrystal water suspensions were prepared from pre-treated fibres by sulphuric acid
113 hydrolysis (Fortunati et al., 2013; Luzi et al., 2014). The hydrolysis was carried out with 64 %wt/wt
114 sulphuric acid at 45 °C for 30 min. After the hydrolysis, a centrifugation (4400 rpm 20 min) and a
115 dialysis procedure (around 5-7 days) were applied in order to remove the excess of acid while a
116 mixed bed ion exchange resin (Dowex Marathon MR-3 hydrogen and hydroxide form) was added
117 to the cellulose suspension for 48 h and then removed by filtration in order to adjust the negative
118 charges induced by the hydrolysis. The resultant cellulose nanocrystal aqueous suspension was
119 ultrasonicated by means of a tip sonicator (Vibracell, 750) for 5 min (Figure 1, Panel B). The final
120 CNC water suspension was approximately 0.5 %wt/wt and the final yield after the hydrolysis was
121 calculated as % of initial weight of the used pre-treated sunflower fibres.
122
123 **2.3 Cellulose nanofibrils extraction**
124 The extraction procedure of cellulose nanofibrils (CNF) was done by a steam explosion treatment
125 that involved 1) alkali treatment with steam explosion; 2) bleaching and 3) mild acid hydrolysis
126 coupled with steam explosion (Figure 1, Panel C). Initially the sunflower stalks were cut into small
127 pieces with grinder. A laboratory autoclave, model no: KAUC-A1 which can work with 137 Pa was
128 used for steam explosion treatment. 100g of ground piece of stalks were treated with 5%wt NaOH
129 solution and kept in an autoclave with the pressure of 137 Pa with the temperature of 180°C in an
130 autoclave for 1.5 hours. After that, a bleaching of the resultant alkali treated stalk sample was done
131 by treating with 5%wt sodium hypochlorite solution for 1.5 hours. Bleaching was repeated six times
132 until the residue become white in colour. After bleaching, the fibres were thoroughly washed, dried
133 and subjected to mild acid hydrolysis using 5% oxalic acid under a pressure of 137 Pa in an

autoclave for 20 minutes. The pressure was released immediately and the process was repeated six times. The fibres were taken out, washed and dispersed in water and homogenized under continuous stirring for 6 hours and the resultant suspension became cellulose nanofiber aqueous suspension. The final product was washed with deionised water by successive centrifugations until neutralization.

2.4 Characterization of CNC and CNF

2.4.1 CNC characterization

The microstructure of CNC was investigated by field emission scanning electron microscopy (FESEM, Supra 25-Zeiss) after gold sputtering, while the shear-induced birefringence of 0.6 %wt CNC solution was analysed in a dark box. For comparison, the microstructure of the cross section and the surface of pristine sunflower stalks and the surface of chemically pre-treated fibres were also investigated by FESEM. The images of the pristine and pre-treated fibres were analysed with the NIS-Elements BR (Nikon) software in order to determine the fibre average diameters.

Fourier infrared (FT-IR) spectra of pristine, chemically pre-treated fibres, and CNC were recorded using a Jasco FT-IR 615 spectrometer in transmission mode while thermogravimetric measurements (TGA) were performed by using a Seiko Exstar 6300 analyser from 30 to 900 °C at 10 °C min^{-1} in nitrogen atmosphere.

2.4.2 CNF characterization

Transmission electron microscopy, JEOL JEM 2100 was used to determine the dimensions of the extracted cellulose nanofibers from the sunflower stalks. A drop of a diluted suspension (0.5 wt %) was deposited on the surface of a clean copper grid and coated with a thin carbon film. The sample was dried at room temperature before TEM analysis and the measurement was carried out with an accelerating voltage of 80 kV.

X- ray equatorial diffraction profiles was used to determine the crystallinity of the sunflower stalks subjected to the different treatments. Each material in the respective treatment was milled into the powder and placed on the sample holder. The diffraction patterns of the raw, alkali treated, bleached and acid treated samples were obtained with an X-ray diffractometer (JEOL diffractometer, Model JDX 8P) using CuK radiation (λ_ = 0.1539 nm) at the operating voltage and current of 40 kV and 20 mA, respectively. The X-ray diffractograms were obtained at room temperature within a 2θ range from 5 to 80° and a scan rate of 2°min^{-1}. The crystallinity index (I_{cr}) of the material was determined by the Segal method as shown in the equation 1 (Segal et al. 1959).

$$I_{cr} = \left\lfloor \frac{I_{002} - I_{am}}{I_{002}} \right\rfloor \times 100 \qquad \text{(Eq. 1)}$$

Where I_{cr} expresses the relative degree of crystallinity, I_{002} is the maximum intensity of the (0 0 2) lattice diffraction at 2θ = 22º, and I_{am} is the intensity of diffraction at 2θ = 18°. I_{002} represents both crystalline and amorphous regions, while I_{am} represents only the amorphous part.

Fourier transform infrared spectra were recorded using a Shimadzu IR-470 IR spectrophotometer. Raw, alkali-treated, bleached, acid-treated fibres and nanocrystals of sunflower stalks samples were analyzed. Prior to the experiment, the samples were dried in an air oven at 60 °C for 12 h. The FT-IR spectrum of each sample was obtained in the range of 400–4000 cm^{-1}. The KBr disk (ultrathin pellets) method was used and the experiments were carried out with a resolution of 2 cm^{-1} and a total of 15 scans for each sample.

2.5 Gluten bionanocomposites preparation

The wheat gluten bionanocomposite films loaded with 1% wt. and 3% wt., respect to the matrix weight, of both CNC (density 1.3 g cm^{-3}) (Mukherjee, Kao, Gupta, Quazi, & Bhattacharya, 2016) and CNF (density 1.5 g cm^{-3}) (Jonoobi, Harun, Mathew, & Oksman, 2010) were prepared by using the method described by Kayseriliolu (Kayserilioglu, Bakir, Yilmaz & Akkas, 2003) with minor

183 modification. The formulations are designed as Gluten_1CNC, Gluten_3CNC, Gluten_1CNF,
184 Gluten_3CNF, respectively (volume fractions of cellulosic materials, CNC or CNF, respect to the
185 gluten volume used for each samples are 0.47% v/v, 1.45% v/v, 0.41% v/v, 1.26% v/v,
186 respectively). Deionized water was mixed with 2 %wt of glycerol as plasticizer. Wheat gluten was
187 dispersed in the prepared solution (10 %wt) with magnetic stirring at high speed. Sodium hydroxide
188 solution (0.5 M) was then carefully added to the solution with magnetic stirring at low speed at
189 room temperature for 30 min, until pH =10.8 was obtained, and a following heating in a water bath
190 at 70 °C for 10 min under controlled pH, was applied. After cooling, specific amounts of both CNC
191 and CNF aqueous dispersions were added and magnetically stirred for 30 min at RT. Finally, the
192 solutions were casted on the *Teflon*® sheet and the drying was performed at RT until films could be
193 easily removed. Gluten based films 90-100 µm thick were obtained. The bionanocomposite films
194 were conditioned before characterization at 20 °C and 53 % relative humidity conditions in
195 desiccators by using a magnesium nitrate-6-hydrate saturated solution (Sigma-Aldrich) for at least
196 one week. Neat gluten based films were also produced for comparison by using the same procedure
197 and the excess of water used for CNC and CNF based formulations was here considered and added.
198
199 **2.6 Characterization of gluten based bionanocomposites**
200 The microstructure of the gluten based bionanocomposite fractured surfaces was investigated by
201 scanning electron microscope, FESEM, after gold sputtering of the surfaces. The surface properties
202 of the produced formulations were investigated by both atomic force microscopy (AFM) and optical
203 microscopy. The AFM analysis was performed by using a Nanoscope III.a Scanning Probe
204 Microscope, (Multimode 8, Bruker AXS, Inc. Santa Barbara, California, USA), with a NanoScope®
205 V controller electronics. Measurements were taken from several areas of the film surface (50 x 50
206 µm and 3 x 3 µm), using the phase imaging mode. Optical analysis was carried out by light
207 microscopy using an optical microscopy (DM/LP Leica Microsystems, Wetziar GmbH) with a CCD

208 camera incorporated, which allowed acquiring images from different samples. Images of films
209 containing or not cellulose nanocrystals were acquired by using x200 magnification.
210 The transparency of the films was determined from the surface reflectance spectra by using a
211 spectrocolorimeter CM-3600d (Minolta Co, Tokyo, Japan) with a 30 mm illuminated sample area
212 by applying the Kubelka–Munk theory for multiple scattering to the reflection spectra. This theory
213 was based on that the light passes through the film, it is partially absorbed and scattered, which is
214 quantified by the absorption (K) and the scattering (S) coefficients. Internal transmittance (T_i) of the
215 films was quantified using equation 2. In this equation, R_0 is the reflectance of the film on an ideal
216 black background. Parameters a and b were calculated by equations 3 and 4, where R is the
217 reflectance of the sample layer backed by a known reflectance R_g. The reflection spectra on the
218 white and black background were determined from 400 to 700 nm. Measurements were taken in
219 triplicate for each formulation.

220 $$T_i = \sqrt{(a - R_0)^2 - b^2} \qquad \text{(Eq. 2)}$$

221

222 $$a = \frac{1}{2}\left(R + \frac{R_0 - R + R_g}{R_0 R_g}\right) \qquad \text{(Eq. 3)}$$

223 $$b = (a^2 - 1) \qquad \text{(Eq. 4)}$$

224 Colour coordinates of the films, L*, C^*_{ab} (equation (5)) and h_{ab} (equation (6)) from the CIELAB
225 colour space were determined using D65 illuminant and 10° observer and taking into account R_∞
226 (equation (7)) which correspond with the reflectance of an infinitely thick layer of the material.

227 $$C^*_{ab} = \sqrt{a^{*2} + b^{*2}} \qquad \text{(Eq. 5)}$$

228 $$h^*_{ab} = arctg\left(\frac{b^*}{a^*}\right) \qquad \text{(Eq. 6)}$$

229 $$R_\infty = a - b \qquad \text{(Eq. 7)}$$

Finally, colour differences between the different films and control film were evaluated by using, equation (8):.

$$\Delta E = \sqrt{(\Delta L^*)^2 + (\Delta a^*)^2 + (\Delta b^*)^2} \qquad \text{(Eq. 8)}$$

Gloss was measured using a flat surface gloss meter (Multi-Gloss 268, Minolta, Langenhagen, Germany) at an incidence angle of 60º, according to the ASTM standard D523 (ASTM, 1999). Gloss measurements were performed over a black matte standard plate and were taken in triplicate. Results were expressed as gloss units, relative to a highly polished surface of standard black glass with a gloss value close to 100.

Thermal characterization was done by both differential scanning calorimetric (DSC) and thermogravimetric analysis (TGA). DSC measurements were carried out on a TA Instruments DSC Q200 in modulated mode (TA Instruments Inc., USA) equipped with Universal Analysis 2000 software. Film samples, weighing 8 ± 1mg, were placed in a hermetically sealed sample pan and tested from −70 to 170 ◦C at a heating rate of 5 °C min^{-1}. The period and the amplitude of modulation were respectively 60 s and 0.50 °C. The glass-rubber transition temperature (T_g) was determined from the temperature at the inflexion point, corresponding to the temperature at which the differential heat flow is maximum. TGA tests (Seiko Exstar 6300) from 30 to 600 °C at 10 °C min^{-1} under a nitrogen atmosphere were performed for each sample.

X-ray diffraction was used to determine the crystallinity of the CNC and CNF gluten composite films with varying concentrations of CNC and CNF. Each film was placed on the sample holder to obtain total and uniform X-ray exposure. The X-ray diffraction patterns of neat gluten, Gluten_1CNC, Gluten_3CNC, Gluten_1CNF and Gluten_3CNF films were obtained with an X-ray diffractometer (SHIMADZU XRD-6000). The x-ray diffractograms were obtained at room temperature within a 2θ range from 5 to 60º and a scan rate of 2°min^{-1}.

253 The mechanical behaviour of gluten based bionanocomposite films was evaluated by tensile tests,
254 performed on rectangular probes (50 mm x 10 mm) on the basis of UNI ISO 527 standard with a
255 crosshead speed of 50 mm min^{-1}, a load cell of 500 N and an initial gauge length of 25 mm. The
256 elastic modulus (E), the tensile strength (σ_b) and elongation at break (ε_b) were calculated from the
257 resulting stress-strain curves. The measurements were done at room temperature and at least five
258 samples were tested.
259 The barrier properties of the gluten based formulations were evaluated by both water vapour
260 permeability (WVP) test and oxygen transmission rate measurements. WVP was evaluated
261 following the gravimetric method ASTM E96-95 (ASTM, 1995) by using Payne permeability cups
262 (Payne, elcometer SPRL, Hermelle/sd Argenteau, Belgium) of 3.5 cm diameter. Deionised water or
263 lithium chloride salt were used inside the testing cups to achieve 100 or 11 % RH respectively, on
264 one side of the film, meanwhile an oversaturated magnesium nitrate solution was used to control the
265 RH (53 % RH) on the other side of the film. The relative humidity of the tests was selected
266 according to the final use of the flexible films as package material, thus simulating the contact with
267 fresh food, such as meat or fresh cut fruit or very low water activity products, respectively. A fan
268 placed on the top of the cup was used to reduce resistance to water vapour transport. Water vapour
269 transmission rate measurements (WVTR) were performed at 25 ºC. To calculate WVTR, the slopes
270 in the steady state period of the weight loss vs. time curves were determined by linear regression.
271 WVP was calculated according to Cano et al., 2014 (Cano, Jiménez, Cháfer, Gónzalez & Chiralt,
272 2014). For each type of film, WVP measurements were taken in quadruplicate.
273 The oxygen barrier capacity of the gluten based bionanocomposite films was evaluated by
274 measuring oxygen permeability (OP) by means of an Ox-Tran 1/50 system (Mocon, Minneapolis,
275 USA) at 25 °C (ASTM Standard Method D3985-95, 2002). Measurements were taken at 53 % in
276 films previously equilibrated at the same RH. Films were exposed to pure nitrogen flow on one side
277 and pure oxygen flow on the other side. The OP was calculated by dividing the oxygen transmission

278 rate by the difference in the oxygen partial pressure on the two sides of the film, and multiplying by
279 the average film thickness. At least three replicates per formulation were taken into account.
280
281 **2.7 Statistical analysis**
282 Results were analysed by analysis of variance (ANOVA), using the Statgraphics Plus 5.1. Program
283 (Manugistics Corp., Rockville, MD). To differentiate samples, Fisher's least significant difference
284 (LSD) was used at the 95 % confidence level.
285
286 **3. Results and Discussion**
287 **3.1. Cellulose nanostructures extracted from sunflower stalks**
288 *3.1.1. Characterization of extracted cellulose nanocrystals*
289 Sunflower stalks present a heterogeneous structure characterized by an external lignocellulosic wall
290 and an interior white core. In this research, we selected only the external fibrous part of the
291 sunflower stalks for CNC extraction. Figure 2 shows the morphological appearance of the raw
292 material (Figure 2 a and b), of the pre-treated fibres (Figure 2 c) and of the novel extracted CNC
293 (Figure 2 d). Figure 2 a shows the porous honeycomb network that characterizes the cross section of
294 sunflower stalks (Marechal & Rigal, 1999; Nozahic & Amziane, 2012), while the surface image
295 confirms their heterogeneous, rough and pitted structure (Figure 2 b).
296 The applied chemical treatment provoked an evident defibrillation process of the sunflower stalks
297 as a consequence of hemicellulose and lignin removal (confirmed by the whitening, Figure 1, Panel
298 A) and the fibres appear well individualized, with a regular, smooth and clean surface (Figure 2 c),
299 while each elementary filament shows a compact structure and very long entangled cellulosic fibrils
300 (Figure 2 c-insert) with a diameter of pre-treated fibres of 12.3±3.1 μm (calculated by FESEM
301 images by the NIS-Elements BR-Nikon software).

Concerning the hydrolysis procedure for the extraction of cellulose nanocrystals, the measured yield of the applied procedure was approximately 21% and this is an important result considering the low cellulose content that characterized the used raw material (about 40% for depithed stalks). The FESEM image (Figure 2d) confirms that the aqueous suspensions containing cellulose nanocrystals consisted mostly of individual crystals with the previously reported acicular structure ranged from 150 to 200 nm in length and 5-10 nm in diameter (aspect ratio 26 ± 10) (Fortunati, Puglia, Luzi, Santulli, Kenny & Torre, 2013), while a 69.8% of crystallinity index was calculated from XRD pattern. Finally, the aqueous suspension exhibited the typical shear-induced birefringence of CNC (Figure 2d-insert), highlighting their ability to form a chiral nematic liquid crystalline phase in equilibrium with the isotropic phase and underlining the success and effectivity of the selective extraction procedure.

The results of thermal and chemical investigations of raw material, pre-treated fibres and CNC are also summarized in Figure 2. The DTG curves (Figure 2e) suggest that the pyrolysis process of pristine fibres can be separated into three main stages: the first weight loss is due to moisture loss, the second is due to the main thermal decomposition of cellulose (centred at 304 °C with a shoulder peak at 225 °C due to hemicellulose and lignin components) (Figen, İsmail & Pişkin, 2012; Varhegyi, Jakab, Till & Szekely, 1989) and the third step is related to the lignin and hemicelluloses decomposition. In the case of pre-treated fibres, the first weight loss was reduced, while the elimination of the shoulder in the second peak of the DTG profile confirmed the elimination of hemicellulose and lignin material by the treatment with sodium hydroxide. Moreover, the shift of the main peak related to cellulose decomposition to higher temperatures indicates an increase of the thermal stability of the pre-treated fibres, due to the reduced amount of non-cellulosic material of the fibre and the presence of high crystalline cellulosic components. In the case of CNC, two well-separated pyrolysis processes are observed in the DTG curves. The first one is likely due to the weaker interaction of single bond OH groups in cellulose that requires less energy to start the

thermal degradation process, while the main DTG peak of the cellulose is shifted to a higher temperature (353 °C) probably due to different ordered and packed cellulose regions, possibly higher crystallite size and therefore higher thermal stability (Flandez, González Tovar, Bayer Resplandis, El Mansouri, Vilaseca Morera & Mutjé Pujol, 2012).

Figure 2f shows the spectra fingerprint region of pristine, pre-treated fibres and CNC extracted from sunflower stalks. The interior part of the sunflower stem is extremely rich in polysaccharides, with OH hydroxyl group stretching leading to a large peak between 3000 and 3600 cm^{-1}. The absorption peak around 2900 cm^{-1} indicates the stretching vibration of C–H band of CH_2 methylene group (2920 and 2850 cm^{-1}), characteristic of waxes and fats (Nozahic & Amziane, 2012). In the case of pre-treated fibres, the signal at 1511 cm^{-1} assigned to the aromatic C-O stretching mode for the guayacyl ring of lignin, disappeared as expected (Monlau, Barakat, Steyer & Carrere, 2012). The spectrum of CNC reported identifiable bands as adsorbed water in cellulose (1641 cm^{-1}) and bands at 1423, 1377, 1339 and 1311 cm^{-1} attributed respectively to CH_2 symmetric bending, CH bending, in-plane OH bending and CH_2 rocking vibration in cellulose. Furthermore, the signals at 1163, 1116, 1061, 1033, 897 cm^{-1} are assigned respectively to asymmetric C-O-C stretching, anhydroglucose ring asymmetric stretching, C-O stretching, in-plane C-H deformation of cellulose can be identified (Chen, Ferrari, Angiuli, Yao, Raspi & Bramanti, 2010).

3.1.2.Characterization of extracted cellulose nanofibrils

Extracted cellulose nanofibers from sunflower stalks were examined by transmission electron microscopy (TEM) to find the dimensions of the nanofibers. From TEM image, Figure 3a, it can be seen that fibres with average diameter in the range of 5-10 nm with a good network were obtained. In other words, a number of branches of small bundles or individualized nanofibers were hooked up to larger aggregates. This TEM image concludes that steam explosion coupled with mild acid hydrolysis is an effective method to produce cellulose nanofibers. The steam explosion treatment

352 was expected to break down the lignocellulosic structure, hydrolyze the hemicellulose fraction and
353 depolymerize lignin components (Cara, Ruiz, Ballesteros, Negro & Castro, 2006; Cara, Ruiz,
354 Ballesteros, Manzanares, 336 Negro & Castro, 2008).
355 Crystallinity of cellulose in each nanofiber is an important factor for determining the mechanical
356 and thermal properties. The ability of cellulose hydroxyl groups to bond each-other play a major
357 role in directing the crystalline packing and also governing the physical properties of cellulose.
358 Cellulose has a well prominent crystalline structure due to hydrogen bonding and van der Waals
359 interactions existing between adjacent cellulose molecules compared to hemicellulose and lignin,
360 which are amorphous in nature. The chemical treatment is one of the governing factors which
361 deeply affect the crystallinity of the cellulose; hence, in order to evaluate the effectiveness of the
362 chemical treatment, crystallinity of the treated fibres can be determined and compared with values
363 for untreated fibre. Figure 3b shows the diffraction patterns obtained for pristine, alkali treated,
364 bleached and acid hydrolysed sunflower stalk samples. It is noticed that there is a gradual increase
365 in crystallinity index at each stage of treatments and it is maximum for acid treated samples. The
366 intense peak in the acid treated sample clearly indicates the efficient removal of non cellulosic
367 polysaccharides and dissolution of amorphous zones (Cherian, Pothan, Nguyen-Chung, Mennig,
368 Kottaisamy & Thomas, 2008). The values of the crystallinity index obtained at different stages of
369 isolation are shown in Figure 3d**.** Crystallinity index showed a gradual increase in crystallinity from
370 initial raw fibre to acid treated nanofiber. The high crystallinity of nanofibers will increase their
371 stiffness and rigidity and it could be more effective in providing better reinforcement for composite
372 materials.
373 FTIR spectroscopy involves the interaction of energy and matter. By recording the magnitude of
374 absorbed energy and comparing it with available database, the present functional groups can be
375 identified and chemical structure of the sample can be characterized. The plant fibre consists of
376 three main materials which include cellulose, hemicellulose and lignin. These materials are mainly

377 composed of alkanes, esters, aromatics, ketones and alcohols with different oxygen containing
378 functional groups. FTIR analysis of the untreated, alkali treated, bleached and acid treated
379 sunflower stalks samples are given in Figure 3c. During isolation process, most of the lignin and
380 hemicelluloses parts have been removed from the fibres. This could be understood from the IR
381 studies. The peak at 3300 cm^{-1}, which was observed in the spectra of all fibres, corresponds to the
382 OH stretching vibrations of hydrogen bonded hydroxyl group and it shows the hydrophilic tendency
383 of the fibre (Karimi, Shafiei & Kumar, 2013; Pelissari, do Amaral Sobral & Menegalli, 2014). The
384 peak at 1630 cm^{-1} is due to the bending mode vibration of the absorbed water with some
385 contributions from carboxylate groups (Chirayil, Mathew & Thomas, 2014). These results indicate
386 that the cellulose component was not removed during the chemical treatment and hence we can
387 conclude that the steam explosion coupled with the mild acid hydrolysis treatment effectively
388 removed the lignin and hemicellulose portions from the fibre matrix.
389
390 *3.1.3.CNC vs CNF*
391 FTIR studies have been done on the extracted cellulose nanofibers and nanocrystals from sunflower
392 stalks. FTIR spectra of cellulose nanofibers and cellulose nanocrystals are shown in the Figure 4a, it
393 is observed that cellulose nanofibers show the band at 896 cm^{-1} which is assigned as β-glucosidic
394 linkage for the cellulose I structure and cellulose nanocrystals shows the band at 894 cm^{-1} position
395 which is due to the cellulose II structure (Gwon, Lee, Chun, Doh & Kim, 2010). The change
396 occurred was due to the rotation of glucose residue around the glucosidic bond (Ray & Sarkar,
397 2001). In addition, it can be seen that band of the cellulose nanofibers at 998 cm^{-1} was shifted to 996
398 cm^{-1} in the case of nanocrystals. This was also related to the transformation from cellulose I to
399 cellulose II crystal structure (Gwon, Lee, Chun, Doh & Kim, 2010). This may be justified by
400 transformation and regeneration of cellulose chains after prolonged chemical treatments. We can

401 conclude that the cellulose nanocrystals and cellulose nanofibers show the structure of cellulose II
402 and cellulose I, respectively.
403 XRD studies were done on both cellulose nanofibers and nanocrystals from sunflower stalks to
404 investigate the effect of chemical purification on crystallinity. Figure 4b shows the X-ray diffraction
405 peaks of both cellulose nanofibers and nanocrystals. The cellulose nanofibers shows diffraction
406 peaks around $2\theta = 16.3°$ and $2\theta = 22.6°$ which typically represent cellulose type I. In the case of
407 cellulose nanocrystals, the pattern was changed to Cellulose II, with a split peak around $2\theta = 20°$
408 and 21.7º (Nasri-Nasrabadi, Mehrasa, Rafienia, Bonakdar, Behzad & Gavanji, 2014). This may be
409 justified by transformation and regeneration of cellulose chains after chemical treatments.
410

411 **3.2. Characterization of gluten based bionanocomposites**

412 *3.2.1. Morphological and transparency properties*

413 The microstructure of the cross-section surfaces of gluten based bionanocomposites was
414 qualitatively analyzed by using FESEM, while the surface structure was analyzed by AFM and
415 optical microscope in order to evaluate the influence of cellulose nanoreinforcements and the
416 modification on the neat gluten microstructure (Figure 5).
417 FESEM images of fractured surface of gluten based nanocomposites show a homogenous aspect
418 with the absence of visible cellulose nanoreinforcements; however, the presence of some holes was
419 detected for Gluten_CNF nanocomposites. A high homogeneity was evidenced for gluten matrix
420 based film that tended to decrease for the nanocomposite systems; in fact, different phases can been
421 seen by FESEM analysis (and then by AFM) both for Gluten_CNC and Gluten_CNF and this
422 effect, more evident for CNF, can be related to the domains of gluten and cellulose
423 nanoreinforcements that were formed during the processing. The production of the holes was, in
424 fact, typically related to the incorporation of air and to the evaporation of the solvents during the

425 casting of the materials, and it was here enhanced by the presence of CNF due to their different
426 morphology and dimensions with respect to CNC (Chevillard et al., 2011).
427 AFM images show the topographic analysis of gluten based bionanocomposites obtained by using
428 Phase Imaging mode derived from Tapping Mode. Phase Imaging allows detecting variations in
429 composition. In gluten and gluten based nanocomposites, heterogeneous response of different phase
430 can be detected. In gluten film the different phases can be related to the presence of gluten and
431 glycerol, while for nanocomposites the different areas can also be related to the presence of the
432 nanoreinforcements. AFM images also underline a good distribution for the CNC into the matrix,
433 whilst CNF agglomerates can be found in Gluten_1CNF; however, this effect is not evident for
434 Gluten_3CNF because the analysed region does not allow identifying CNF agglomerates.
435 Optical microscope images of film surfaces for the Gluten_CNF show a clear presence of
436 heterogeneous materials due to the agglomeration of long nanofibrils created during the processing
437 or cast phase identifiable as brown areas. The aggregation phenomenon is more evident for
438 Gluten_3CNF. The presence of aggregates and holes negatively influences not only the morphology
439 of the material but also its optical, barrier, and mechanical properties.
440 Table 1 shows the values of internal transmittance (T_i) at 450 nm, the gloss values at 60° and the
441 values of the colorimetric analysis of gluten and gluten bionanocomposites. According to Kubelka -
442 Munk theory, high values of T_i are associated to structural homogeneity and their degree of
443 transparency, while low T_i values are related to a high structural heterogeneity and greater opacity.
444 The highest T_i value was found for Gluten_3CNC and for the other gluten based bionanocomposites
445 the values of transparency remain unchanged with respect to gluten film (Table 1). A significant
446 difference ($p<0.05$) was obtained between Gluten_3CNC and the other four formulations.
447 The gloss of bionanocomposites was greatly affected by the presence of nanoreinforcements. In the
448 case of bionanocomposites reinforced with CNC, the values of gloss increase as a function of filler
449 percentage. The opposite behaviour was evidenced for the nanocomposites reinforced with CNF; in

this case, the gloss decreases at the higher filler content. This result can be related to the presence of agglomerates on the surface of Gluten_CNF, as also evidenced by optical microscopy. In the case of Gluten_CNC, the nanoreinforcements are homogeneously distributed into the matrix while, as shown in Figure 5, in the Gluten_CNF nanocomposites the surfaces show the presence of agglomerates related at the presence of CNF.

The colour of the bionanocomposites is a consequence of the colour of gluten powder and it is expressed in term of lightness (L^*), chroma (C_{ab}^*), hue (h_{ab}^*). Incorporation of CNC or CNF in gluten films induced very small colour changes. CNC provoked a less saturated (lower chroma values) and less yellow (lower hue values) colour in gluten films, whereas CNF induce a more saturated and yellow colour. The total colour differences ΔE were estimated between the neat gluten and bionanocomposites. Since the ΔE values between the neat gluten and bionanocomposites were lower than 2, these are in the limit of the human eye perception (Mahy, et al. 1994). To conclude, optical parameters are largely related to films microstructure, finishing degree, and degree of roughness.

3.2.2. Thermal physical properties

Results of TGA tests are reported in Figure 6 a and Table 2. During thermal degradation under nitrogen flow, the gluten based materials containing CNC and CNF have shown a four steps-decomposition pattern, which corresponds, respectively, to the elimination of moisture, glycerol evaporation, degradation of cellulosic nanoreinforcements and decomposition of wheat gluten. The first peak below 100°C in DTG curves can be attributed to water evaporation, while the second step, in which there was a further weight loss, occurred after the elimination of moisture and corresponded to the evaporation of glycerol. As reported in Table 2, the $DTG_{II\ peak}$ moved to higher temperatures with increasing content of CNC from 0 to 3% wt. (from 248 to 251 and 252 °C, respectively for Gluten_1CNC and Gluten_3CNC). This was believed to be due to the preferable

barrier property of CNC well dispersed in gluten matrix, which could efficiently delay the evaporation of glycerol or water vapour moisture. In the case of cellulose nanofibers, we observed a shift towards lower temperatures (from 248 to 239 and 228 °C, respectively for Gluten_1CNF and Gluten_3CNF), indicating in this case a less stable structure. CNF consists of both individual and aggregated nanofibrils made of alternating crystalline and amorphous cellulose domains, with a different ordered and packed cellulose regions with respect of rigid CNC, that indeed present a higher crystallinity index than the others, due to the disruption of amorphous holocellulose surrounding and embedding the cellulose crystallites formed by well organized glucose chains (Wang, Sain & Oksman, 2007). The neat gluten maximum degradation was registered at 317 °C (Mojumdar, Moresoli, Simon & Legge, 2011) and similar temperatures have been measured for DTG_{max} values (see Table 2) in the case of films containing CNC (316 and 315 °C, respectively for Gluten_1CNC and Gluten_3CNC); a shift towards lower temperatures was registered for the Gluten_CNF at the two different weight percent (310 and 307 °C, respectively for Gluten_1CNF and Gluten_3CNF). A decrease of maximum degradation rate related to the main peak was observed in the case of CNC containing gluten (from 0.089 $\mu g\ \mu g_i\ min^{-1}$ for neat gluten to 0.070 $\mu g\ \mu g_i^{-1}\ min^{-1}$ and 0.055 $\mu g\ \mu g_i^{-1}\ min^{-1}$, for Gluten_1CNC and Gluten_3CNC, respectively), indicating an effective action of CNC as barrier to diffusion of degradation products from the bulk of the gluten polymer to the gas phase. The same behaviour was not revealed in CNF containing gluten films, that nevertheless showed similar values for degradation rate peaks with increasing CNF content. The measured values of residual mass at the final temperature of the test (800 °C) (see Table 2) showed that addition of CNC and CNF slightly influenced the measurement. The small increase in char formation for cellulose nanocrystals and cellulose nanofibrils could be due to two reasons: (1) the sulphate group acts as a dehydration catalyst and facilitates the char residue formation (Kim, Nishiyama, Wada & Kuga, 2001), or (2) owing to their small particle size, a large number of free end chains is present which trigger decomposition at lower temperature and

consequently increasing the yield of char (Staggs, 2006). The results of T_g measurements from modulated DSC heating scan (reversible heat flow) of wheat gluten bionanocomposites are also reported in Table 2. The registered high-temperature peak is associated with the glass transition of the plasticized gluten phase (high-T_g) (Rafieian, Shahedi, Keramat & Simonsen, 2014a). The values for T_g increase from 107.9 °C to 111.8 °C with increase of CNC content from 0 to 3 %wt. Even in the case of CNF reinforcement, we obtained a shift of the glass transition to higher temperature, but the increase was less evident in the case of gluten films containing cellulose nanofibrils at the two different weight percents, in particular no further increase was registered at 3 %wt of CNF. This result suggests the strong increasing interactions between CNC and gluten matrix in the gluten rich phase, which restricts the mobility of the motion of gluten chain segments and elevates the glass transition temperature with increasing content of CNC and CNF (Song & Zheng, 2009). In the case of wheat gluten bionanocomposites reinforced with CNF, the partial increase could be due to the limiting effect of CNF in restricting the mobility of the plasticized protein chain for a decreased plasticization effect of water due to a re-distribution of cellulose–water interactions within the matrix (Roohani, Habibi, Belgacem, Ebrahim, Karimi & Dufresne, 2008).

X-ray diffraction patterns were obtained for the neat wheat gluten and gluten bionanocomposite films of various wt. % of CNC and CNF. Figure 6 b shows X-ray diffraction patterns of the neat gluten and that of bionanocomposite films. From the figure, it can be clearly shown that neat wheat gluten showed no crystallinity on its x-ray diffraction pattern due to its non-crystalline nature (Lim and Fujio 1989). In the case of Gluten_CNF composites films, the x-ray diffraction pattern showed a prominent peak around $2\theta = 22.6°$, indicating the presence of cellulose I CNF, whereas Gluten_CNC composite films showed two small peaks around $2\theta=20°$ and 21.7°, indicating the presence of cellulose II CNC.

3.2.3. Mechanical and barrier properties

Table 2 shows barrier and mechanical properties evaluated for gluten based nanocomposites (90-100 μm thick). The barrier characterization is one of the most important requirements for food packaging. The goal of food packaging is twofold: to contain the food and to decrease its contamination with the surrounding atmosphere, increasing its shelf-life (Rhim, Park & Ha, 2013). Incorporation of CNC and CNF slightly modify OP of gluten films, depending on their morphology and ratio. The lowest ratio of CNC reduced OP, whereas at the highest ratio reinforcements tend to increase OP, as for CNF. This effect can be attributed to the aggregation degree of the reinforcement material (depending on their ratio in the films), which was more intense in the case of CNF, as previously commented. The presence of particles increases the tortuosity factor for mass transfer through the polymer (Fortunati, Peltzer, Armentano, Jimenez & Kenny, 2013), reducing permeability values, but the aggregation phenomenon and the induced morphology (presence of some holes) provoke a reduction of tortuosity factor, leading to OP values nearer to the gluten matrix.

The water vapour permeability was evaluated at 25 °C and at two different conditions of relative humidity, the first one at 11-53% RH and the second one at 100-53 %RH.

The WVP analysis, at 11-53% RH gradient, show a significant reduction of the permeability coefficients for CNC composites, around 34 and 32% for Gluten_1CNC and Gluten_3CNC respectively, although no significant effect of CNF on WVP was observed. This behaviour can also be related to the ability of CNC to increase the tortuous path of water molecules through the nanocomposite structure (Fortunati et al., 2014), while the greater aggregation degree of CNF reduced the capacity of reinforcement to limit permeation of water molecules. However, at 100-53% RH gradient, no significant differences among WVP values of gluten and bionanocomposite films were observed, probably due to the greater plasticization degree of the polymer matrix, which implied a sharp increase in the permeation capacity of water molecules. In this situation, the potential barrier effect of reinforcements was clearly inhibited, in line with the moisture gain of the

550 hydrophilic gluten matrix and the subsequent increase in the molecular mobility and the rate of all
551 diffusion dependent processes. Therefore, it is evident that gluten films should be only used as food
552 packaging for dry foods because high humidity compromises the stability of films.
553 Tensile tests of gluten and gluten based bionanocomposite films were performed at room
554 temperature and the results are summarized in Table 2. All studied bionanocomposite formulations,
555 both Gluten_CNC and Gluten_CNF based films, showed Young's modulus higher than neat gluten
556 (300 MPa), and significant increase was induced by the presence of both cellulosic nanostructures
557 (CNC and CNF), highlighting their reinforcement effect. Moreover, the highest value of Young's
558 modulus was registered for Gluten_1CNC. Cellulose nanocrystals are known to form a percolating
559 network within the polymer matrix in which the stress is assumed to be transferred through
560 crystal/crystal interaction and crystal/polymer matrix interaction (Fortunati et al., 2012). This result
561 confirms again the strong interactions between CNC and gluten matrix. On the contrary, no
562 particular changes were detected in tensile strength and elongation at break values with the presence
563 of either CNC or CNF in gluten matrix.
564
565 **4. Conclusions**
566 Gluten based bionanocomposites reinforced with cellulose based nanofillers extracted from
567 sunflower stalks were prepared by solvent casting technique. Two types of nanostructured fillers
568 were used: cellulose nanofibrils (CNF) and cellulose nanocrystals (CNC).
569 Cellulose nanocrystals (150-200 nm in length and 10 nm in diameter) were successfully extracted
570 from sunflower stalks by an acid hydrolysis with a relatively high yield (21%), while a steam
571 explosion treatment that involved alkali treatment with steam explosion, bleaching and mild acid
572 hydrolysis coupled with steam explosion, was successfully applied, allowing the CNF extraction.
573 The chemical characterization of CNC and CNF underlined that cellulose nanocrystals and cellulose
574 nanofibrils showed the structure of cellulose II and cellulose I, respectively.

575 After the extraction procedures, the obtained cellulosic nanomaterials, both CNC and CNF, were
576 embedded in gluten natural matrix by using a sustainable and low cost water casting procedure.
577 FESEM investigations highlighted that gluten based bionanocomposites showed a homogenous
578 morphology, with the absence of visible cellulose nanoreinforcements; the presence of some holes
579 induced by the processing procedure and more evident for Gluten_CNF nanocomposites, was
580 detected, affecting the optical properties and the gloss of the studied formulations. The different
581 morphology and consequent dispersion of the cellulosic materials into the gluten matrix also
582 affected the barrier properties of the produced bionanocomposite formulations. CNC were, in fact,
583 more efficient in reducing the permeability to gases, due to their ability to increase the tortuous path
584 of gas molecules. On the contrary, the presence of some CNF agglomerates, as shown by optical
585 microscopic images of Gluten_CNF based systems, negatively affected the barrier properties of
586 these formulations, especially with the oxygen and in the case of the highest content of cellulose
587 nanofibrils. Finally, the results of mechanical investigations underlined that all the studied
588 bionanocomposite formulations, both Gluten_CNC and Gluten_CNF films, showed Young's
589 modulus higher than neat gluten, highlighting the effect of reinforcement exerted by both CNC and
590 CNF when embedded in gluten natural matrix, more evident for CNC.
591 The proposed study suggested the possibility to re-valorise agricultural wastes, such as sunflower
592 stalks, by the extraction of added value high-performance cellulosic materials with potential
593 applications as reinforcement in natural polymer based bionanocomposites.
594

595 **Acknowledgments**

596 The authors acknowledge Coldiretti Terni (Italy) and Dr. Aleano Barbarossa for sunflower supply.
597

598 **References**

599 Akpinar, O., Levent, O., Sabanci, S., Uysal, R.S., Sapci B. (2011). Optimization and comparison of
600 dilute acid pretreatment of selected agricultural residues for recovery of xylose. *Bioresouces*, 6(4)
601 4103.
602 Berglund, D.R. (2007). *Sunflower Production*. North Dakota Agricultural Experiment Station and
603 North Dakota State University Extension Service. North Dakota State University Fargo, North
604 Dakota 58105.
605 Cano, A., Jiménez, A., Cháfer, M., Gónzalez, C., & Chiralt, A. (2014). Effect of amylose:
606 amylopectin ratio and rice bran addition on starch films properties. *Carbohydrate Polymers, 111*,
607 543-555.
608 Cara, C., Ruiz, E., Ballesteros, I., Negro, M. J., & Castro, E. (2006). Enhanced enzymatic
609 hydrolysis of olive tree wood by steam explosion and alkaline peroxide delignification. *Process*
610 *Biochemistry, 41*(2), 423-429.
611 Cara, C., Ruiz, E., Ballesteros, M., Manzanares, P., Negro, M. J., & Castro, E. (2008). Production
612 of fuel ethanol from steam-explosion pretreated olive tree pruning. *Fuel, 87*(6), 692-700.
613 Chaker, A., Alila, S., Mutjé, P., Vilar, M. R., & Boufi, S. (2013). Key role of the hemicellulose
614 content and the cell morphology on the nanofibrillation effectiveness of cellulose pulps. *Cellulose*,
615 *20*(6), 2863-2875.
616 Chen, H., Ferrari, C., Angiuli, M., Yao, J., Raspi, C., & Bramanti, E. (2010). Qualitative and
617 quantitative analysis of wood samples by Fourier transform infrared spectroscopy and multivariate
618 analysis. *Carbohydrate Polymers, 82*(3), 772-778.
619 Cherian, B. M., Pothan, L. A., Nguyen-Chung, T., Mennig, G., Kottaisamy, M., & Thomas, S.
620 (2008). A novel method for the synthesis of cellulose nanofibril whiskers from banana fibers and
621 characterization. *Journal of Agricultural and Food Chemistry, 56*(14), 5617-5627.

622 Chevillard, A., Angellier-Coussy, H., Cuq, B., Guillard, V., César, G., Gontard, N., & Gastaldi, E.
623 (2011). How the biodegradability of wheat gluten-based agromaterial can be modulated by adding
624 nanoclays. *Polymer Degradation and Stability, 96*(12), 2088-2097.
625 Chirayil, C. J., Mathew, L., & Thomas, S. (2014). Review of recent research in nano cellulose
626 preparation from different lignocellulosic fibers. *Reviews on Advanced Materials Science, 37*, 20-
627 28.
628 Domenek, S., Feuilloley, P., Gratraud, J., Morel, M.-H., & Guilbert, S. (2004). Biodegradability of
629 wheat gluten based bioplastics. *Chemosphere, 54*(4), 551-559.
630 Díaz, M. J., Cara, C., Ruiz, E., Pérez-Bonilla, M., & Castro, E. (2011). Hydrothermal pre-treatment
631 and enzymatic hydrolysis of sunflower stalks. *Fuel, 90*(11), 3225-3229.
632 Figen, A., İsmail, O., & Pişkin, S. (2012). Devolatilization non-isothermal kinetic analysis of
633 agricultural stalks and application of TG-FT/IR analysis. *Journal of Thermal Analysis and*
634 *Calorimetry, 107*(3), 1177-1189.
635 Flandez, J., González Tovar, I., Bayer Resplandis, J., El Mansouri, N.-E., Vilaseca Morera, F., &
636 Mutjé Pujol, P. (2012). Management of corn stalk waste as reinforcement for polypropylene
637 injection moulded composites. *BioResources, 7, (2), 1836-1849.*
638 Fortunati, E., Armentano, I., Zhou, Q., Iannoni, A., Saino, E., Visai, L., Berglund, L. A., & Kenny,
639 J. M. (2012). Multifunctional bionanocomposite films of poly(lactic acid), cellulose nanocrystals
640 and silver nanoparticles. *Carbohydrate Polymers, 87*(2), 1596-1605.
641 Fortunati, E., Peltzer, M., Armentano, I., Jimenez, A., & Kenny, J. M. (2013). Combined effects of
642 cellulose nanocrystals and silver nanoparticles on the barrier and migration properties of PLA nano-
643 biocomposites. *Journal of Food Engineering, 118*(1), 117-124.
644 Fortunati, E., Puglia, D., Luzi, F., Santulli, C., Kenny, J. M., & Torre, L. (2013). Binary PVA bio-
645 nanocomposites containing cellulose nanocrystals extracted from different natural sources: Part I.
646 *Carbohydrate Polymers, 97*(2), 825-836.

Fortunati, E., Puglia, D., Monti, M., Peponi, L., Santulli, C., Kenny, J. M., & Torre, L. (2013). Extraction of Cellulose Nanocrystals from Phormium tenax Fibres. *Journal of Polymers and the Environment, 21*(2), 319-328.

Fortunati, E., Rinaldi, S., Peltzer, M., Bloise, N., Visai, L., Armentano, I., Jimenez, A., Latterini, L., & Kenny, J. M. (2014). Nano-biocomposite films with modified cellulose nanocrystals and synthesized silver nanoparticles. *Carbohydrate Polymers, 101,* 1122-1133.

Gwon, J. G., Lee, S. Y., Chun, S. J., Doh, G. H., & Kim, J. H. (2010). Effects of chemical treatments of hybrid fillers on the physical and thermal properties of wood plastic composites. *Composites Part A: Applied Science and Manufacturing, 41*(10), 1491-1497.

Jonoobi, M., Harun, J., Mathew, A.P., Oksman, K. (2010). *Composites Science and Technology*, 70, 1742-1747.

Jung, C.-D., Yu, J.-H., Eom, I.-Y., & Hong, K.-S. (2013). Sugar yields from sunflower stalks treated by hydrothermolysis and subsequent enzymatic hydrolysis. *Bioresource Technology, 138*(0), 1-7.

Karimi, K., Shafiei, M., & Kumar, R. (2013). Progress in physical and chemical pretreatment of lignocellulosic biomass. *Biofuel Technologies* (pp. 53-96): Springer.

Kayserilioglu, B. S., Bakir, U., Yilmaz, L., & Akkas, N. (2003). Drying temperature and relative humidity effects on wheat gluten film properties. *Journal of Agricultural and Food Chemistry, 51*(4), 964-968.

Khristova, P., Bentcheva, S., Karar, I. (1998). Soda-AQ pulp blends from kenaf and sunflower stalks. *Bioresource Technology*, 66(2), 99-103.

Kim, D.-Y., Nishiyama, Y., Wada, M., & Kuga, S. (2001). High-yield carbonization of cellulose by sulfuric acid impregnation. *Cellulose, 8*(1), 29-33.

Kopania, E., Wietecha, J., Chiechanska, D. (2012). Studies on Isolation of cellulose fibers from waste plant biomass. *Fibres and Texiles in estarn Europe*, 20, 6B (96), 167-172.

672 Luzi, F., Fortunati, E., Puglia, D., Lavorgna, M., Santulli, C., Kenny, J. M., & Torre, L. (2014).
673 Optimized extraction of cellulose nanocrystals from pristine and carded hemp fibres. *Industrial*
674 *Crops and Products, 56*(0), 175-186.
675 Mahy, M., Eycken, L., Oosterlinck, A., (1994). Evaluation of uniform color spaces developed after
676 the adoption of CIELAB and CIELUV. *Color Research & Application,* 19 (2),105-121.
677 Marechal, V., & Rigal, L. (1999). Characterization of by-products of sunflower culture –
678 commercial applications for stalks and heads. *Industrial Crops and Products, 10*(3), 185-200.
679 Mojumdar, S. C., Moresoli, C., Simon, L. C., & Legge, R. L. (2011). Edible wheat gluten (WG)
680 protein films: preparation, thermal, mechanical and spectral properties. *Journal of Thermal Analysis*
681 *and Calorimetry, 104*(3), 929-936.
682 Monlau, F., Barakat, A., Steyer, J. P., & Carrere, H. (2012). Comparison of seven types of thermo-
683 chemical pretreatments on the structural features and anaerobic digestion of sunflower stalks.
684 *Bioresource Technology, 120*(0), 241-247.
685 Mukherjee, T., Kao, N., Gupta, R.K., Quazi,N., Bhattacharya, S. (2016). Evaluating the state of
686 dispersion on cellulosic biopolymer by rheology. Journal of Applied Polymers Science, doi:
687 10.1002/APP.43200.
688 Nasri-Nasrabadi, B., Mehrasa, M., Rafienia, M., Bonakdar, S., Behzad, T., & Gavanji, S. (2014).
689 Porous starch/cellulose nanofibers composite prepared by salt leaching technique for tissue
690 engineering. *Carbohydrate Polymers, 108,* 232-238.
691 Nozahic, V., & Amziane, S. (2012). Influence of sunflower aggregates surface treatments on
692 physical properties and adhesion with a mineral binder. *Composites Part A: Applied Science and*
693 *Manufacturing, 43*(11), 1837-1849.
694 Pelissari, F. M., do Amaral Sobral, P. J., & Menegalli, F. C. (2014). Isolation and characterization
695 of cellulose nanofibers from banana peels. *Cellulose, 21*(1), 417-432.

Rafieian, F., Shahedi, M., Keramat, J., & Simonsen, J. (2014a). Mechanical, thermal and barrier properties of nano-biocomposite based on gluten and carboxylated cellulose nanocrystals. *Industrial Crops and Products, 53*, 282-288.

Rafieian, F., Shahedi, M., Keramat, J., & Simonsen, J. (2014b). Thermomechanical and morphological properties of nanocomposite films from wheat gluten matrix and cellulose nanofibrils. *Journal of Food Science, 79*(1), N100-N107.

Ray, D., & Sarkar, B. K. (2001). Characterization of alkali-treated jute fibers for physical and mechanical properties. *Journal of Applied Polymer Science, 80*(7), 1013-1020.

Rhim, J.-W., Park, H.-M., & Ha, C.-S. (2013). Bio-nanocomposites for food packaging applications. *Progress in Polymer Science, 38*(10), 1629-1652.

Roohani, M., Habibi, Y., Belgacem, N. M., Ebrahim, G., Karimi, A. N., & Dufresne, A. (2008). Cellulose whiskers reinforced polyvinyl alcohol copolymers nanocomposites. *European Polymer Journal, 44*(8), 2489-2498.

Ruiz, E., Cara, C., Manzanares, P., Ballesteros, M., & Castro, E. (2008). Evaluation of steam explosion pre-treatment for enzymatic hydrolysis of sunflower stalks. *Enzyme and Microbial Technology, 42*(2), 160-166.

Ruiz, E., Romero, I., Moya, M., Cara, C., Vidal, J.D., Castro, E. (2013). Dilute sulfuric acid pretreatment of sunflower stalks for sugar production. Bioresource Technology, 140, 292–298.

Song, Y., & Zheng, Q. (2009). Structure and properties of methylcellulose microfiber reinforced wheat gluten based green composites. *Industrial Crops and Products, 29*(2), 446-454.

Staggs, J. E. J. (2006). Discrete bond-weighted random scission of linear polymers. *Polymer, 47*(3), 897-906.

Tunc, S., Angellier, H., Cahyana, Y., Chalier, P., Gontard, N., & Gastaldi, E. (2007). Functional properties of wheat gluten/montmorillonite nanocomposite films processed by casting. *Journal of Membrane Science, 289*(1), 159-168.

721 Vaithanomsat, P., Chuichulcherm, S., & Apiwatanapiwat, W. (2009). Bioethanol Production from
722 Enzymatically Saccharified Sunflower Stalks Using Steam Explosion as Pretreatment *International*
723 *Scholarly and Scientific Research & Innovation* 3(1), 88-91.
724 Varhegyi, G., Jakab, E., Till, F., & Szekely, T. (1989). Thermogravimetric-mass spectrometric
725 characterization of the thermal decomposition of sunflower stem. *Energy & Fuels, 3*(6), 755-760.
726 Wang, B., Sain, M., & Oksman, K. (2007). Study of structural morphology of hemp fiber from the
727 micro to the nanoscale. *Applied Composite Materials, 14*(2), 89-103.
728

729 **Figure and table captions**

730 **Figure 1:** Scheme of the extraction procedure of cellulose nanocrystals: *Panel A*: Sunflower stalks
731 chemical pre-treatment. *Panel B*: CNC extraction. *Panel C*: Scheme of the extraction procedure of
732 cellulose nanofibers by steam explosion coupled with mild acid hydrolysis.
733 **Figure 2:** Morphological appearance of raw material (a and b), pre-treated fibres (c) and novel
734 extracted CNC (d, and d-insert: birefringence image of CNC solution). DTG curves (e) and FT-IR
735 spectra (f) of pristine, pre-treated fibres and extracted CNC.
736 **Figure 3:** Characterization of CNF extracted by steam explosion: TEM (a), XRD (b), FTIR (c) and
737 crystallinity values (d).
738 **Figure 4:** CNC *vs* CNF: FTIR (a) and XRD (b) analyses.
739 **Figure 5:** Morphological investigation of gluten based nanocomposites.
740 **Figure 6:** Thermal properties (a, DTG curves) and XRD (b) analyses of gluten based
741 nanocomposites.
742

743 **Table 1:** Internal transmittance (Ti) at 450 nm, gloss values at 60º and colour coordinates for gluten
744 based bionanocomposites.
745 **Table 2:** Thermal, mechanical and barrier properties of gluten based bionanocomposites.

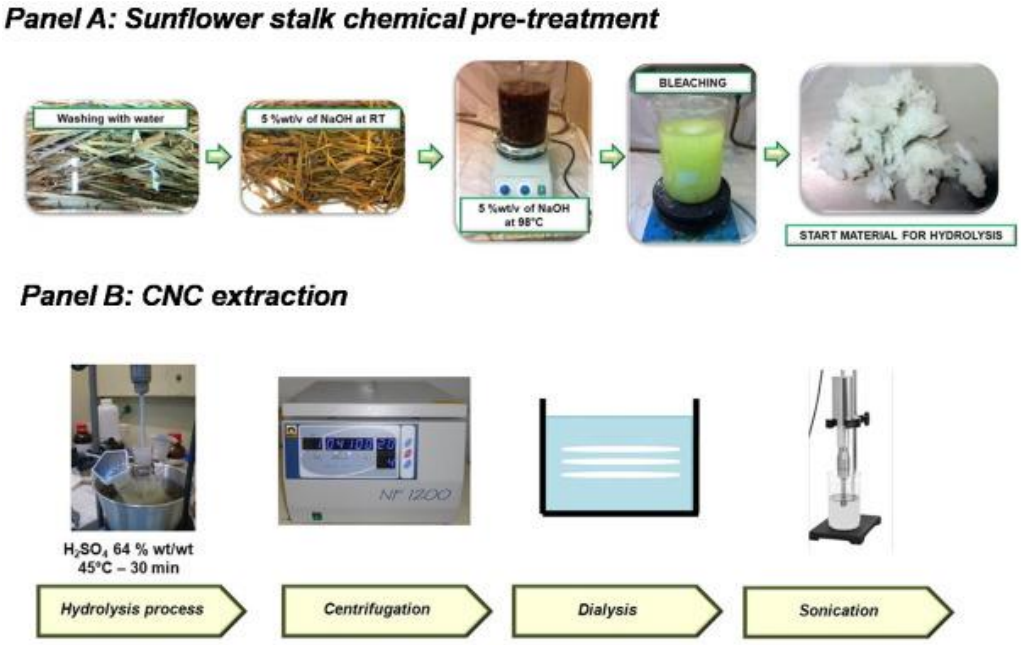
Panel A: Sunflower stalk chemical pre-treatment
Washing with water
5 %wt/v of NaOH at RT
5 %wt/v of NaOH at 98°C
BLEACHING
START MATERIAL FOR HYDROLYSIS
Panel B: CNC extraction
H_2SO_4 64 % wt/wt
45°C – 30 min
Hydrolysis process
Centrifugation
Dialysis
Sonication
Panel C: CNF extraction
Alkali and bleaching Treatment
Removal of Lignin and Hemicellulose
Remain Slurry
Mild acid hydrolysis coupled with steam explosion
Homogenization
CNF Suspension
Cellulose Nanofibers with diameter of 20 nm

746

Figure 1

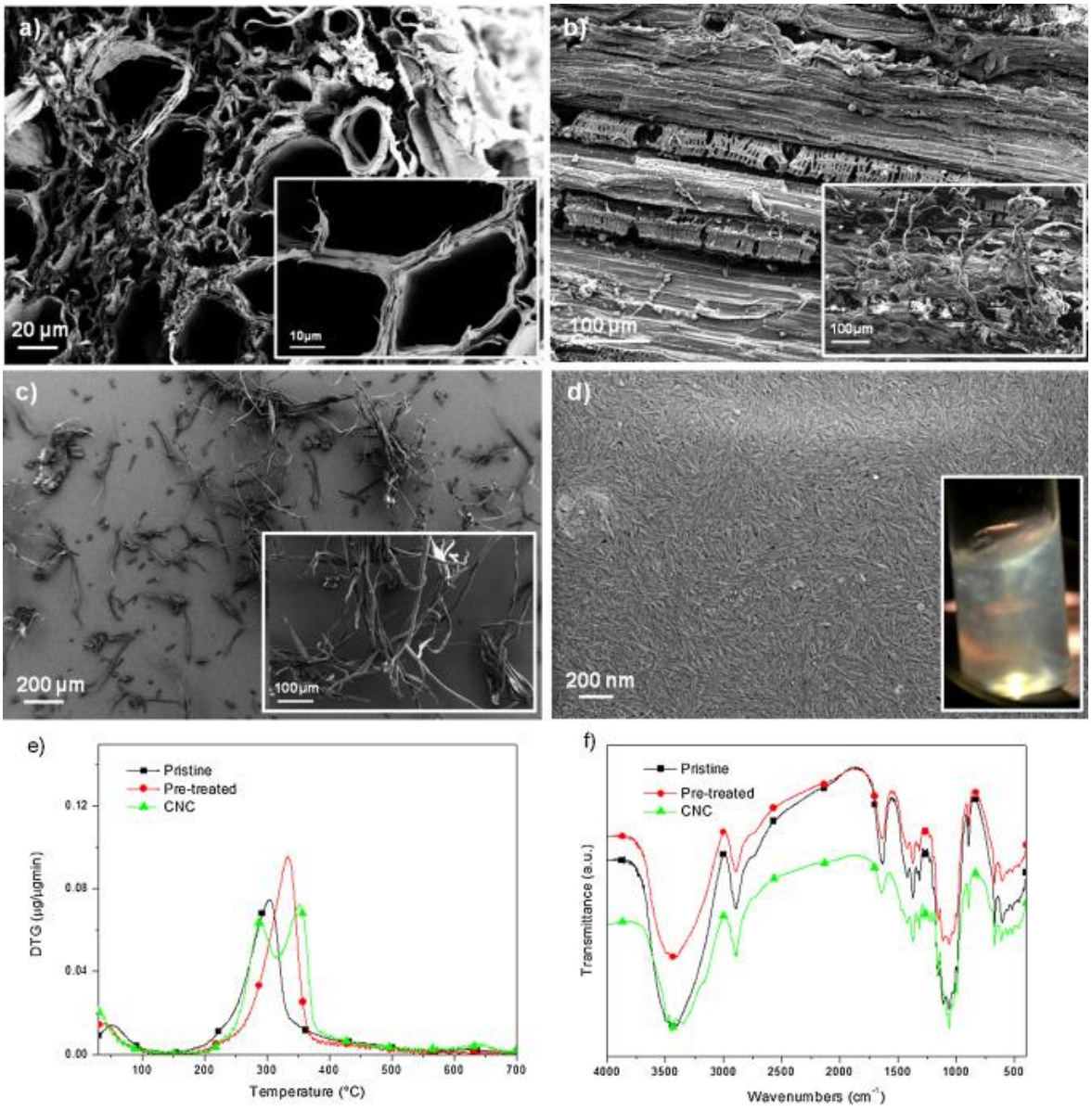
a)
20 µm
10µm
b)
100 µm
100µm
c)
200 µm
100µm
d)
200 nm
e)
Pristine
Pre-treated
CNC
DTG (µg/µgmin)
0.12
0.08
0.04
0.00
100
200
300
400
500
600
700
Temperature (°C)
f)
Pristine
Pre-treated
CNC
Transmittance (a.u.)
4000
3500
3000
2500
2000
1500
1000
500
Wavenumbers (cm-1)

Figure 2

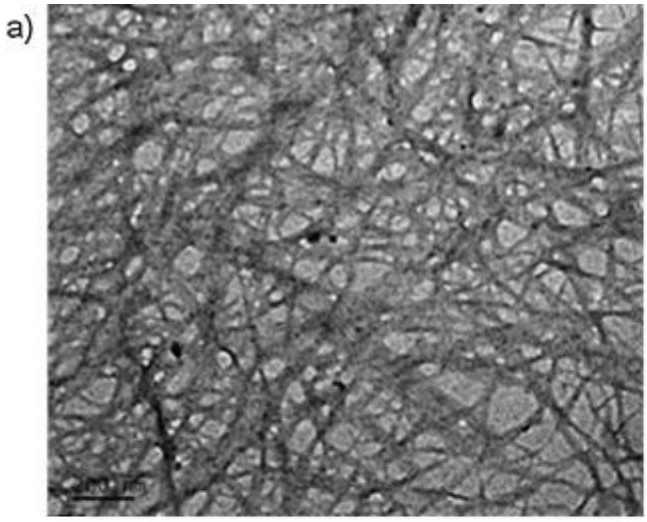

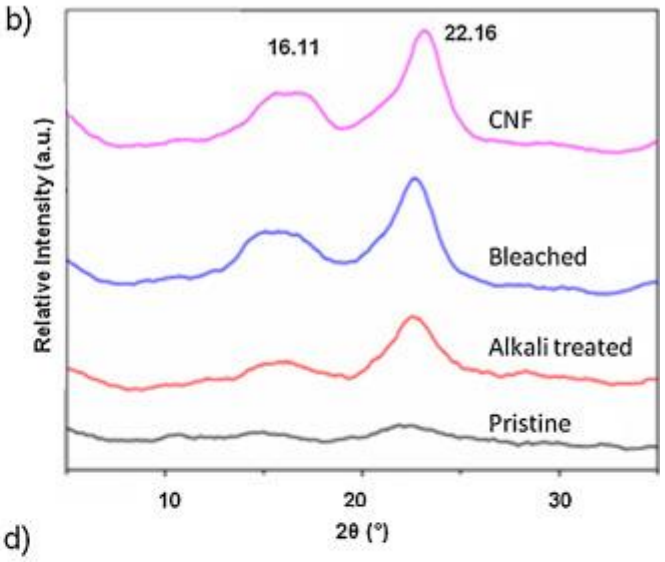

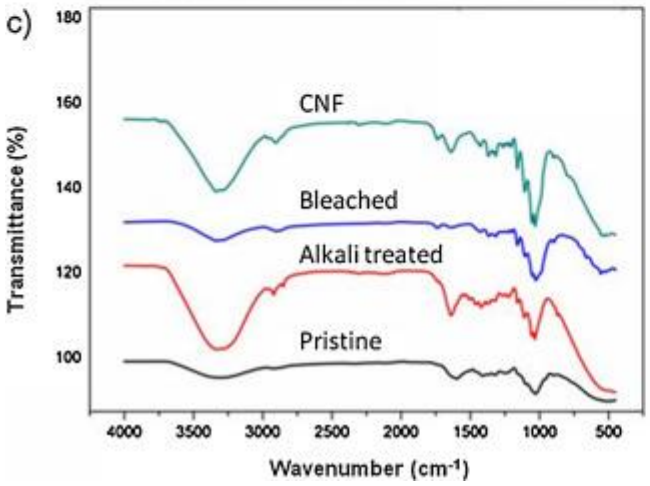

d)

Fiber	Crystallinity Index (%)
Pristine	31.6
Alkali treated	52.7
Bleached	89.1
CNF	93.7

Figure 3

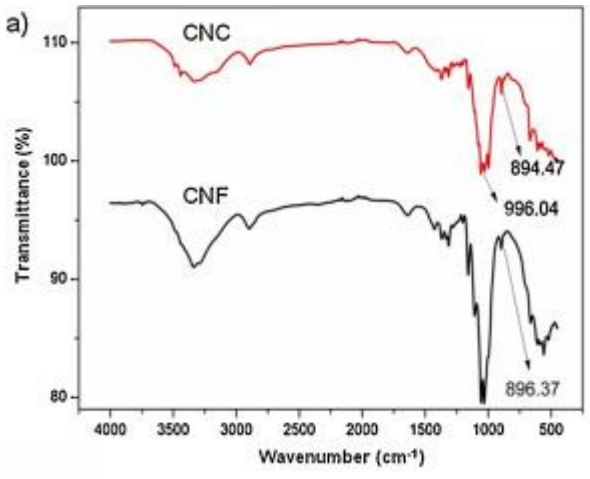

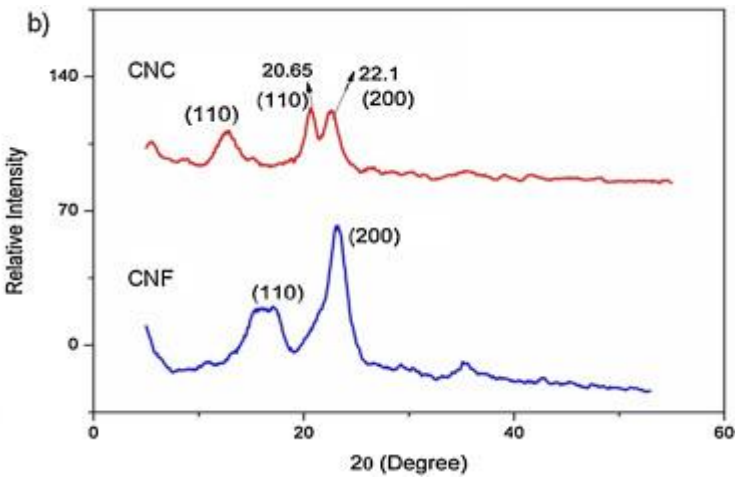

Figure 4

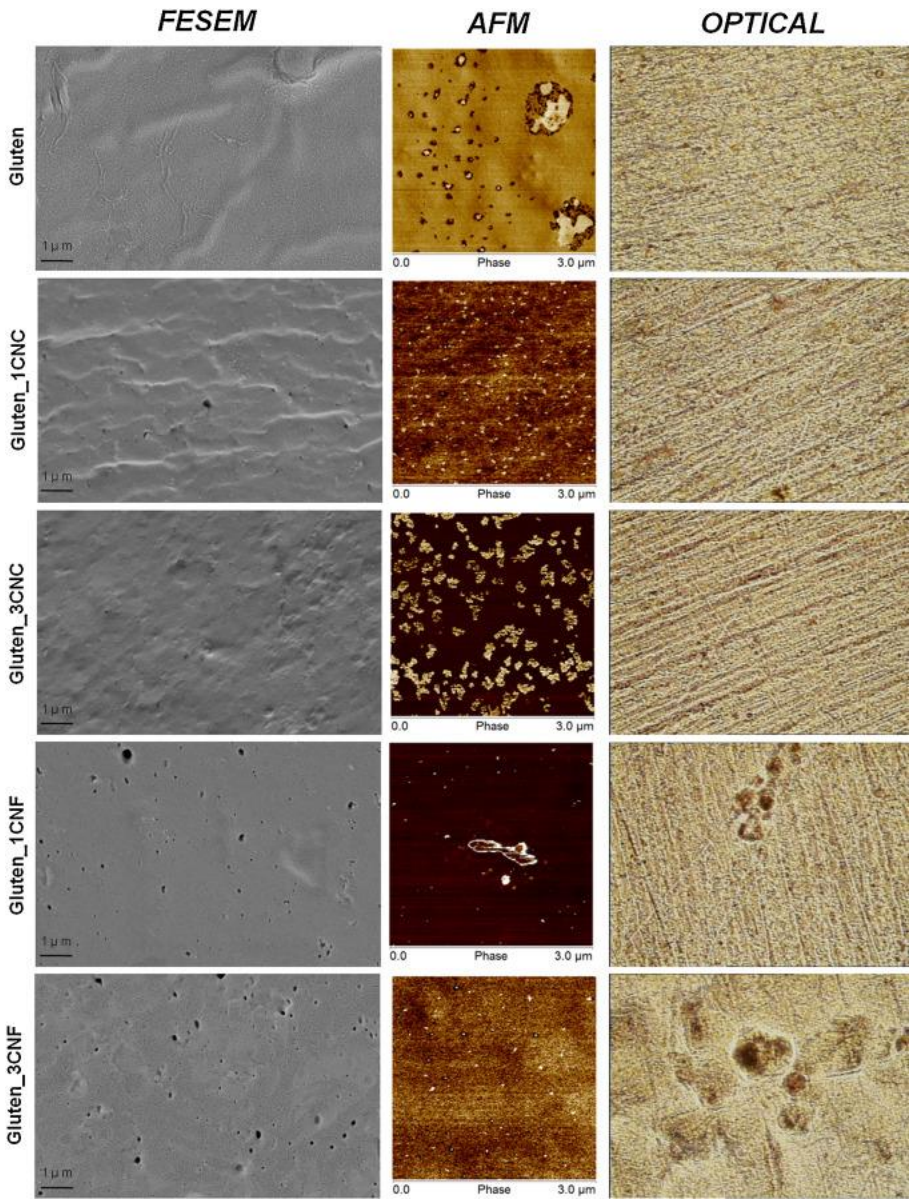
FESEM
AFM
OPTICAL
Gluten
Gluten_1CNC
Gluten_3CNC
Gluten_1CNF
Gluten_3CNF
1 µm
0.0
Phase
3.0 µm

Figure 5

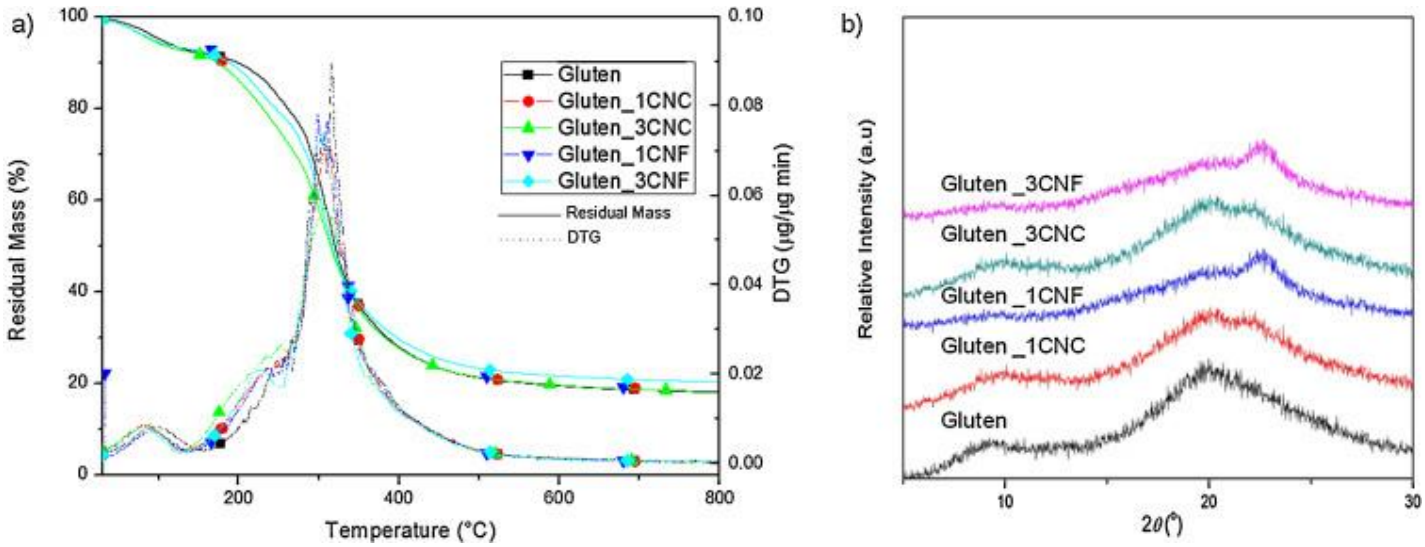

Figure 6

Table 1. Internal transmittance (T_i) at 450 nm, gloss values at 60° and colour coordinates for gluten based bionanocomposites.

Formulations	**Internal transmittance**	**Gloss Values**	**Colour Coordinates**			
Empty Cell	**T_i (450 nm)**	**Gloss 60°**	**L^***	**C^***	**h^***	**ΔE^***
Gluten	58.5 ± 1.3^{a}	54.64 ± 1.56^{a}	65.88 ± 0.71^{ab}	23.94 ± 0.02^{c}	87.64 ± 0.27^{c}	–
Gluten_1CNC	60.7 ± 1.7^{a}	58.03 ± 1.32^{a}	66.60 ± 0.17^{a}	23.44 ± 0.05^{b}	87.58 ± 0.16^{c}	0.087
Gluten_3CNC	64.1 ± 1.5^{b}	64.00 ± 5.99^{d}	67.22 ± 0.66^{b}	23.02 ± 0.07^{a}	86.44 ± 0.20^{a}	1.69
Gluten_1CNF	59.6 ± 0.6^{a}	49.96 ± 1.73^{b}	65.86 ± 0.37^{a}	23.49 ± 0.08^{b}	86.94 ± 0.24^{ab}	0.53
Gluten_3CNF	60.7 ± 0.5^{a}	21.50 ± 1.11^{c}	66.97 ± 0.37^{ab}	24.11 ± 0.13^{c}	87.14 ± 0.43^{bc}	1.12

Different superscripts within the same column indicate significant differences among formulations ($p < 0.05$).

Table 2. Thermal properties, mechanical and barrier properties of gluten based bionanocomposites.

Formulations	Thermal properties			
	DTG_{IIpeak} (°C)	DTG_{max} (°C)	Residual mass (%) at 800 °C	T_g (°C)
Gluten	248	317	18.0	107.9 ± 0.1^{a}
Gluten_1CNC	252	316	18.5	109.4 ± 0.4^{b}
Gluten_3CNC	251	315	18.2	111.8 ± 0.4^{c}
Gluten_1CNF	239	310	18.5	109.7 ± 0.5^{bc}
Gluten_3CNF	228	307	20.3	109.7 ± 0.7^{c}

	Barrier properties		
	OP ($cm^3\ m^{-1}\ s^{-1}\ Pa^{-1}$) 10^{13}	WVP (11–53% RH) (g mmk $Pa^{-1}\ h^{-1}\ m^{-2}$)	WVP (100–53% RH) (g mmk $Pa^{-1}\ h^{-1}\ m^{-2}$)
Gluten	1.210 ± 0.087^{ab}	0.071 ± 0.003^{a}	5.214 ± 0.467^{a}
Gluten_1CNC	1.000 ± 0.0296^{c}	0.047 ± 0.008^{b}	5.037 ± 0.036^{a}
Gluten_3CNC	1.07 ± 0.036^{ac}	0.048 ± 0.005^{b}	5.607 ± 0.514^{a}
Gluten_1CNF	1.080 ± 0.105^{ac}	0.063 ± 0.007^{a}	5.000 ± 0.400^{a}
Gluten_3CNF	1.370 ± 0.145^{b}	0.065 ± 0.002^{a}	5.572 ± 0.290^{a}

	Mechanical properties		
	σ_b (MPa)	ε_b (%)	E_{Young} (MPa)
Gluten	10.7 ± 1.1^{a}	100 ± 30^{a}	300 ± 40^{a}
Gluten_1CNC	12.8 ± 2.6^{a}	100 ± 30^{a}	500 ± 60^{c}
Gluten_3CNC	10.1 ± 1.8^{a}	100 ± 30^{a}	440 ± 60^{bc}
Gluten_1CNF	12.9 ± 2.2^{a}	70 ± 20^{a}	410 ± 60^{bc}
Gluten_3CNF	10.9 ± 2.1^{a}	70 ± 10^{a}	400 ± 70^{ab}

Different superscripts within the same column indicate significant differences among formulations ($p < 0.05$).